shortening of the C–C bond, calculated at 1.426 Å (1.434 Å 6311 G** MP_2), this revealing a significative delocalization. The above calculation and correlation diagram (Figure 2) agree with the attribution of the first band (10.1 eV) to the ionization of the sulfur lone pair interacting with the $n^{\perp}_{C\equiv N}$ orbital. Any vibrational structure should be expected as weak, the ground-state valence vibration $\nu_{C=S}$ being calculated at 1078 cm^{-1}, and was not observed.

The two ionic states of symmetry A″, calculated to lie at 11.56 eV (11.65) and 14.46 eV (15.00), arise respectively from the ejection of an electron from the delocalized orbitals between the two fragments CS and CN (antisymmetric and symmetric interaction $\pi_{CS} - \pi_{CN}$, $\pi_{CS} + \pi_{CN}$). In the experimental spectrum, we assign the bands at 11.8 and 14.1 eV to these two ionic states.

The three other well-resolved bands arise from ionization into σ radical cation states. The band at 12.8 eV with a vibrational progression of 1900 cm^{-1} is unambiguously associated with the orbital in the plane of the CN group. The ionizations at 13.7 and 15.2 eV therefore correspond to those of the σ_{C-S} orbital and of the cyano group lone pair n_N, respectively.

The relative stability of thioformyl cyanide (**1**) and the formation of only minor amounts of carbon disulfide and hydrogen cyanide at a FVT temperature of 1300 K led us to perform an ab initio calculation (3-21G**) of the unimolecular decomposition pathway of this compound. The results (Figure 3) have been determined at the SCF level but remain comparable, considering the involved energetical and geometrical modifications, to those obtained for formyl cyanide.[6] The stationary point is characterized by a Hessian with one negative eigenvalue. The structure of the transition state shows marked lengthening of the C–C bond and decrease of the CCH angle, accompanied by shortening of the C–S bond. The transition-state energy, calculated to be 405.00 $kJ \cdot mol^{-1}$ above compound **1**, appears especially high. Furthermore, the final state leading to the formation of CS and HCN is energetically less stable than **1**.

These theoretical results support our experimental findings that, under dilute gaseous conditions, thioformyl cyanide (**1**) is relatively stable, its unimolecular decomposition process being thermodynamically disfavored. In contrast, formyl cyanide is unstable and decomposes under the same conditions.[5]

Theoretical Studies of Inorganic and Organometallic Reaction Mechanisms. 7. Ab Initio Potential Energy Surfaces of CO Substitutions on Six-Coordinate *trans*-$W(CO)_4(NO)Cl$ and $Re(CO)_5Cl$

Jun Song and Michael B. Hall*

Contribution from the Department of Chemistry, Texas A&M University, College Station, Texas 77843-3255. *Received August 10, 1992*

Abstract: Carbonyl substitution reactions on *trans*-$W(CO)_4(NO)Cl$ and isoelectronic $Re(CO)_5Cl$ were investigated through the construction of ab initio potential energy surfaces. Hartree–Fock–Roothaan calculations for the substitution by PMe_3 on $W(CO)_4(NO)Cl$ predict an associative mechanism with a 7-coordinate intermediate, in which the W–N–O angle is bent to 135.7°. The Laplacian of the total charge density displays a process in which electrons shift from the metal to the nitrogen, create an additional N lone pair, and vacate a coordinate site for the entering ligand. For a weaker donor, such as PH_3, this associative mechanism is not available because poor donors cannot stabilize an intermediate with a bent W–N–O bond. Substitution by any PR_3 in $Re(CO)_5Cl$ also proceeds by a dissociative or I_d mechanism, since here the CO ligand cannot accommodate an additional electron pair and it resists bending to maintain a strong Re–C bond. We also explored the influences of electron correlation and basis set on the potential energy surfaces.

Introduction

Ligand substitution at a transition-metal center is a basic organometallic reaction as well as a crucial step in homogeneous catalytic reactions. Thus, detailed knowledge about the mechanism of such reactions is of particular significance. As good chemical models, the kinetics of substitution reactions of the CO group in the metal carbonyl derivatives have been studied extensively.[1] Among the metal carbonyl derivatives, metal nitrosyl carbonyls continue to receive attention because their novel associative mechanism results in a rapid substitution rate. For instance, although 4-coordinate $Ni(CO)_4$ slowly undergoes substitution through a dissociative mechanism,[2] its isoelectronic analogs $Co(CO)_3(NO)$,[3] $Fe(CO)_2(NO)_2$,[4] and $Mn(CO)(NO)_3$[5] readily react through an associative process. Carbonyl substitutions of 5-coordinate $Fe(CO)_5$[6] and 6-coordinate $Cr(CO)_6$[7] occur by a dissociative mechanism, while their isoelectronic counterparts $Mn(CO)_4(NO)$[8] and $V(CO)_5(NO)$[9] react by an associative pathway. Recent studies on $W(CO)_4(NO)X$ (X = Cl, Br, or I) show that CO substitution proceeds through an associative route with strong nucleophiles such as $P(n\text{-}Bu)_3$ but through a dissociative or intermediate dissociative mechanism for weaker nucleophiles such as PPh_3.[10] This associative pathway apparently is not accessible

(1) For review, see: (a) Howell, J. A. S.; Burkinshaw, P. M. *Chem. Rev.* **1983**, *83*, 557. (b) Basolo, F. *Inorg. Chim. Acta* **1985**, *100*, 33. (c) Basolo, F. *Polyhedron* **1990**, *9*, 1503.
(2) (a) Basolo, F.; Wojcicki, A. *J. Am. Chem. Soc.* **1961**, *83*, 5290. (b) Day, J. P.; Pearson, R. G.; Basolo, F. *Ibid.* **1968**, *90*, 6927.
(3) Thorsteinson, E. M.; Basolo, F. *J. Am. Chem. Soc.* **1966**, *88*, 3929.
(4) Morris, D. E.; Basolo, F. *J. Am. Chem. Soc.* **1968**, *90*, 2531.
(5) Shen, J. K.; Gao, Y. C.; Shi, Q. Z.; Basolo, F. *Inorg. Chem.* **1989**, *28*, 4304.
(6) Wawersik, H.; Basolo, F. *J. Am. Chem. Soc.* **1967**, *89*, 4626.
(7) Graham, J. R.; Angelici, R. J. *Inorg. Chem.* **1967**, *6*, 2082.
(8) Wawersik, H.; Basolo, F. *J. Am. Chem. Soc.* **1967**, *89*, 4626.
(9) Shi, Q. Z.; Richmond, T. G.; Trogler, W. C.; Basolo, F. *Inorg. Chem.* **1984**, *23*, 957.
(10) Sulfab, Y.; Basolo, F.; Rheingold, A. L. *Organometallics* **1989**, *8*, 2139.

0002-7863/93/1515-327$04.00/0

to the isoelectronic metal carbonyl $Re(CO)_5X$.[11]

The explanation for a low-energy, associative mechanism is not obvious at first; a 20-electron transition state/intermediate should be very high energy since organometallic compounds follow the 18-electron rule.[12] However, if the metal complex can shift a pair of electrons onto one of its ligands, then the associative reaction could occur through an 18-electron transition state/intermediate. Because the nitrosyl ligand is such a strong π acceptor, it can easily accommodate an additional electron pair. Thus, a metal orbital can be vacated for an incoming ligand if the nitrosyl bends and converts a metal–ligand bonding pair to a nitrogen lone pair as in eq 1.[3,4] Although quite a few kinetic experiments

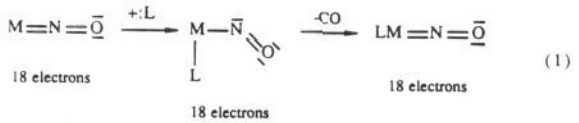

(1)

support an associative mechanism, no direct evidence for the presumed 18-electron high-coordinate transition state/intermediate with a bent nitrosyl is available.

In contrast to extensive ab initio calculations on stable equilibrium structures of organometallic complexes, few investigations have been devoted to understanding the mechanism of organometallic reactions.[13] The characterization of these reactions by potential energy surfaces still remains challenging and is far from routine. Therefore, a detailed theoretical description of the mechanism of CO substitution on metal nitrosyl carbonyls is significant both from the experimental and from the theoretical points of view.

By constructing the potential energy surfaces from ab initio calculations, we attempt to clarify the following questions. For metal nitrosyl carbonyls, does the low-energy pathway involve the bending of the nitrosyl ligand? If so, how much bending is necessary? Why is the associative mechanism only seen with some nucleophiles? What other factors affect the structure and energy of the transition state/intermediate? Does a stable intermediate with a bent nitrosyl exist, or has the bending simply stabilized a transition state? In order to emphasize the role of the nitrosyl ligand in the associative mechanism, we will also investigate the CO substitution on the corresponding isoelectronic metal carbonyl complex.

Calculational Details

Models. $W(CO)_4(NO)Cl$ and $Re(CO)_5Cl$ were utilized as model compounds for the metal nitrosyl carbonyls and the isoelectronic metal carbonyls, respectively. PH_3 and PMe_3 were used as the nucleophiles. The two reaction models are shown in **1** and **2**. In model **1**, PR_3 is short for PH_3 and PMe_3.

Since the interest of this work is in the effect of nitrosyl bending and the relative changes in geometry and energy that occur during the reaction, the following approximations have been employed to simplify the geometry optimizations. In the calculations, models **1** and **2** were restricted to C_s symmetry, i.e., atoms W (or Re), Cl, and P and ligands NO (or C_NO_N), C_cO_c, and C_tO_t were constrained in the mirror plane. Standard geometries[14] were adopted for PR_3 (R = H or Me) groups. Except for the C_NO_N ligand in **2**, all of the CO ligands were set to a linear geometry with a fixed C–O bond length.[15] Except as specified, the metal–Cl and metal–C_ν (ν = t, 1, 2) bond lengths in **1** and **2** were fixed at the corresponding experimental values,[16,17] since the variations

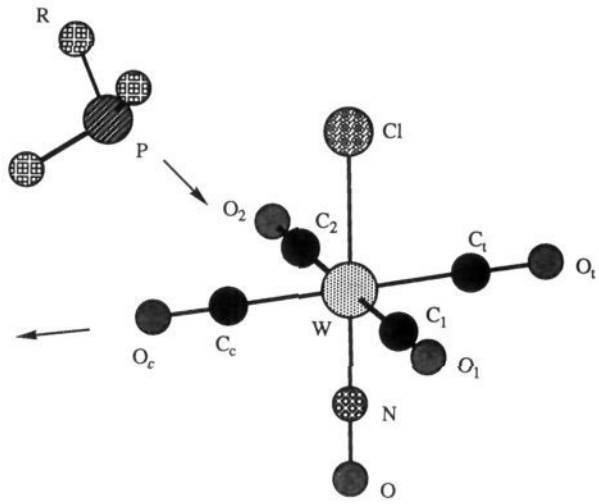

R = H, Me

1

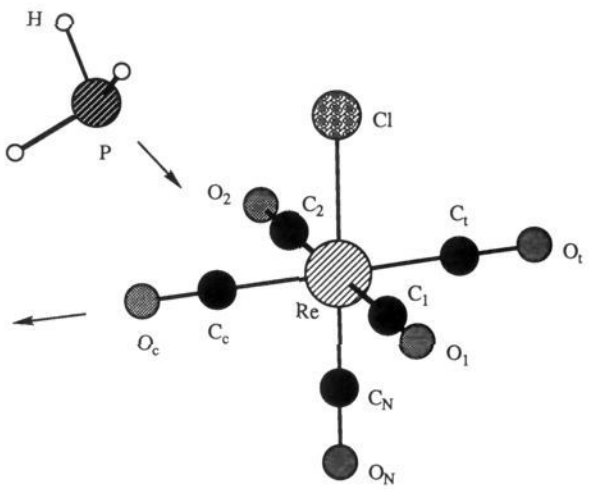

2

of the bond lengths of these spectator ligands are less important during the reaction.

Potential energy surfaces were constructed on coordinates R_1 and R_2, which are defined as

$$R_1 = R_{\text{metal–C}} - R_{\text{metal–P}} \quad (2)$$

$$R_2 = R_{\text{metal–C}} + R_{\text{metal–P}} \quad (3)$$

where $R_{\text{metal–C}}$ and $R_{\text{metal–P}}$ are the distances from the metal atom to the leaving ligand and the entering ligand, respectively. In the construction of these surfaces, 20–30 points were calculated by fixing R_1 and R_2 while optimizing the other geometric variables, as discussed above.

Methods. Ab initio calculations were carried out with restricted Hartree–Fock–Roothaan (RHF) methods.[18] Full-gradient techniques were utilized for geometry optimizations. Electron correlation effects were considered with configuration interaction methods at the level of all single and double excitations (CISD). The RHF and CISD calculations were performed with the GAMESS[19] program package. The topological analysis of the total charge density was performed with the

(11) Brown, D. A.; Sane, R. T. *J. Chem. Soc. A* **1971**, 2088.
(12) Tolman, C. A. *Chem. Soc. Rev.* **1972**, *1*, 337.
(13) Hay, P. J. In *Transition Metal Hydrides*; Alain Dedieu, Ed.; VCH Publishers: New York, 1992; p 127 and references therein. Koga, N.; Morokuma, K. In *Transition Metal Hydrides*; Alain Dedieu, Ed.; VCH Publishers: New York, 1992; p 185 and references therein.
(14) Hehre, W. J.; Ditchfield, R.; Stewart, R. F.; Pople, J. A. *J. Chem. Phys.* **1970**, *52*, 2769.
(15) The value was set to the average of the C–O bond lengths (1.174 Å) in $[(PhMe_2)_2W(NO)(CO)_2I]$ (see ref 10).
(16) The W–C bond distances were fixed to the average of the W–C bond lengths (1.945 Å) in $[(PhMe_2)_2W(NO)(CO)_2I]$ (see ref 10). The W–Cl bond length (2.489 Å) was determined through shortening the W–I bond in $[(PhMe_2)_2W(NO)(CO)_2I]$ by the difference value between the C–I and C–Cl bond lengths in CH_3I and CH_3Cl. The Re–C and Re–Cl bond lengths were directly taken from ref 17.
(17) Cotton, F. A.; Daniels, L. M. *Acta Crystallogr.* **1983**, *C39*, 1495.
(18) (a) Roothaan, C. C. J. *Rev. Mod. Phys.* **1951**, *23*, 69. (b) Roothaan, C. C. J. *Rev. Mod. Phys.* **1960**, *32*, 179.
(19) Guest, M. F. Daresbury Laboratory, Warrington, WA4 4AD, U.K.

Table I. Relative Energies (in kcal/mol) and ρ_c (in e/au^3) for the CO Substitution by PMe_3 in $W(CO)_4(NO)Cl$ along the Associative Pathway

	reactant	early transition state	intermediate	late transition state	product
energy	0.0	19.1	16.4	20.5	-17.0
ρ_c[a]	0.165	0.143	0.103	0.136	0.166

[a] Electron density at the critical point on W-N bond path.

use of Bader's theory,[20] which has been incorporated into the MOPLOT program.[21]

Basis Sets. The core electrons of W (Re) were fitted to an effective core potential, where the 5s and 5p electrons were treated explicitly as valence electrons of W (Re) (ECP 2). The valence electrons were represented with a double-ζ basis, (541/41/21) for W and Re, as described by Hay and Wadt.[22] For carbon in CO ligands, oxygen, phosphorus, nitrogen, and chloride, the effective core potentials and basis sets of Stevens, Basch, and Krauss were employed.[23] Except as specified, double-ζ forms were used for the basis sets of phosphorus and the atoms in the NO, C_cO_c, and C_NO_N ligands, while single-ζ forms were used for the basis sets of the spectator ligands Cl, C_1O_1, C_2O_2, and C_1O_1. The basis set for carbon in the PMe_3 group was the minimum basis set form of Huzinaga.[24] The basis set of hydrogen was an STO-3G representation.[25]

Results and Discussions

CO Substitution by PMe_3 in $W(CO)_4(NO)Cl$. The calculations on the potential energy surface were carried out in the region proximate to an associative species. The dissociative region was also included in the potential energy surface by extending the value of the coordinate $R_2 = R_{metal-C} + R_{metal-P}$. The corresponding contour plot and a part of the potential energy surface are shown in Figure 1.

A local minimum is observable on the potential energy surface. Because both the entering and leaving ligands are close to the metal center, this local minimum represents a seven-coordinate intermediate. Two saddle points which correspond to the early and late transition states are also observed. The reaction coordinate, which connects the reactant, early transition state, intermediate, late transition state, and product, characterizes an associative reaction pathway. Table I shows the energy change along this associative pathway.

In the long-range region of R_2, such as point d on the contour plot of Figure 1, the reaction system dissociates into three fragments, where both the entering and leaving ligands are far from the metal center. In this dissociative region, the energy is higher than that of the early transition state by 6 kcal/mol. Therefore, for this reaction at this level of theory, the associative mechanism is favored over the dissociative one.

Along the associative pathway, we reoptimized five important structures, the reactant, the early and late transition states, the intermediate, and the product. In these optimizations, we dealt with the W–P and W–C_c bond distances in the following way. For the reactant and product we set the W–P and W–C_c distances to 6.0 Å, respectively. For the transition states we fixed the W–P and W–C_c distances to the values obtained from the contour plot (Figure 1). To get a more accurate structure for the intermediate,

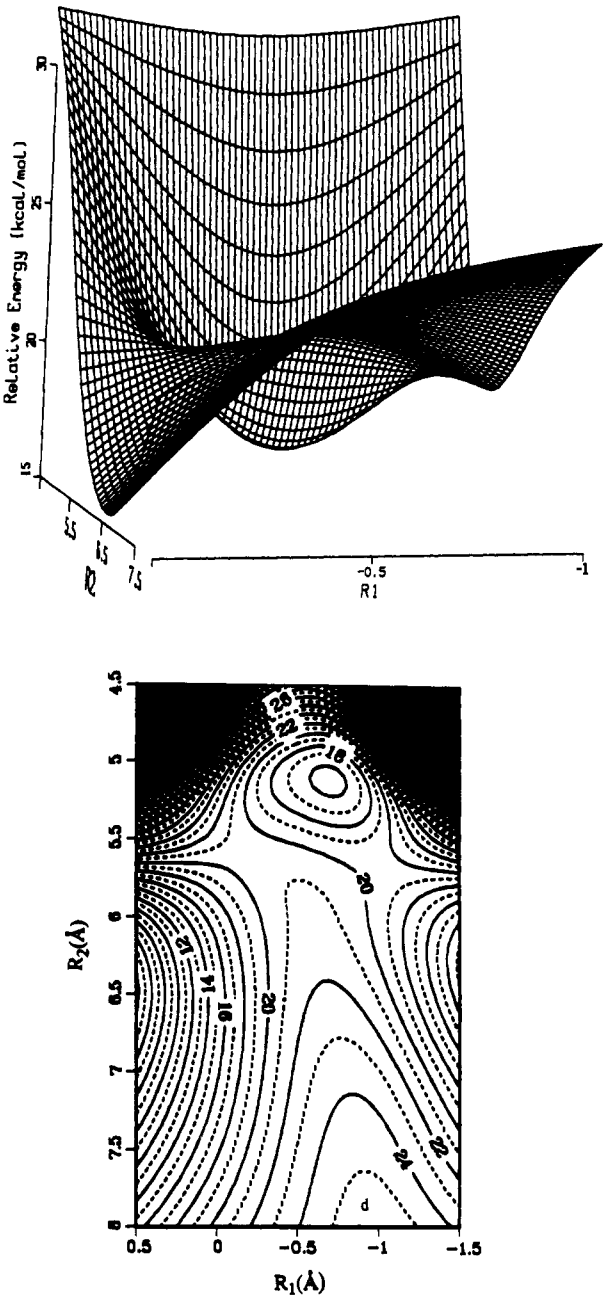

Figure 1. Potential energy surface and contour plot for the CO substitution by PMe_3 in $W(CO)_4(NO)Cl$ as a function of the R_1 and R_2 distances. Energies are in units of kcal/mol. The reactants enter from the far right (negative R_1) and the products leave on the far left (large R_1).

we relaxed both the W–P and the W–C_c bond lengths during the optimization. The optimized structures are presented in Figure 2.

In the course of the reaction, a notable structural change takes place in the NO ligand. As the PMe_3 approaches the metal, the NO begins to bend and the W–N bond lengthens. At the intermediate, the NO bond is most strongly bent, with a W–N–O bond angle of 135.7°, and the W–N bond is at its maximum length of 2.084 Å. In the last stage of the reaction, the NO ligand returns to a linear geometry and the W–N bond shortens. The coincident appearance of the intermediate and the bending of NO suggests that the distortion of the NO ligand plays a key role in the formation of a stable intermediate and in lowering the barrier for the associative mechanism.

Since the structural change of the NO ligand may involve substantial redistribution of the electron density as indicated in

(20) (a) Bader, R. F. W.; Essen, H. *J. Chem. Phys.* **1984**, *80*, 1943. (b) Bader, R. F. W.; MacDougall, P. J.; Lau, C. D. H. *J. Am. Chem. Soc.* **1984**, *106*, 1594.

(21) Interactive MOPLOT: a package for the interactive display and analysis of molecular wave functions incorporating the program MOPLOT (Lichtenburger, D.), PLOTDEN (Bader, R. F. W.; Kenworthy, D. J.; Beddal, P. M.; Runtz, G. R.; Anderson, S. G.), SCHUSS (Bader, R. F. W.; Runtz, G. R.; Anderson, S. G.; Biegler-Koenig, F. W.), and EXTREM (Bader, R. F. W.; Biegler-Koenig, F. W.), Sherwood, P.; MacDougall, P. J. 1989.

(22) Hay, P. J.; Wadt, W. R. *J. Chem. Phys.* **1985**, *82*, 270.

(23) Stevens, W. J.; Basch, H.; Krauss, M. *J. Chem. Phys.* **1984**, *81*, 6026.

(24) Huzinaga, S.; Andzelm, J.; Klobukowski, M.; Radzio-Andzelm, E.; Sakai, Y.; Tatewaki, H. *Gaussian Basis Sets for Molecular Calculations*; Elsevier: New York, 1984.

(25) Hehre, W. J.; Stewart, R. F.; Pople, J. A. *J. Chem. Phys.* **1969**, *51*, 2657.

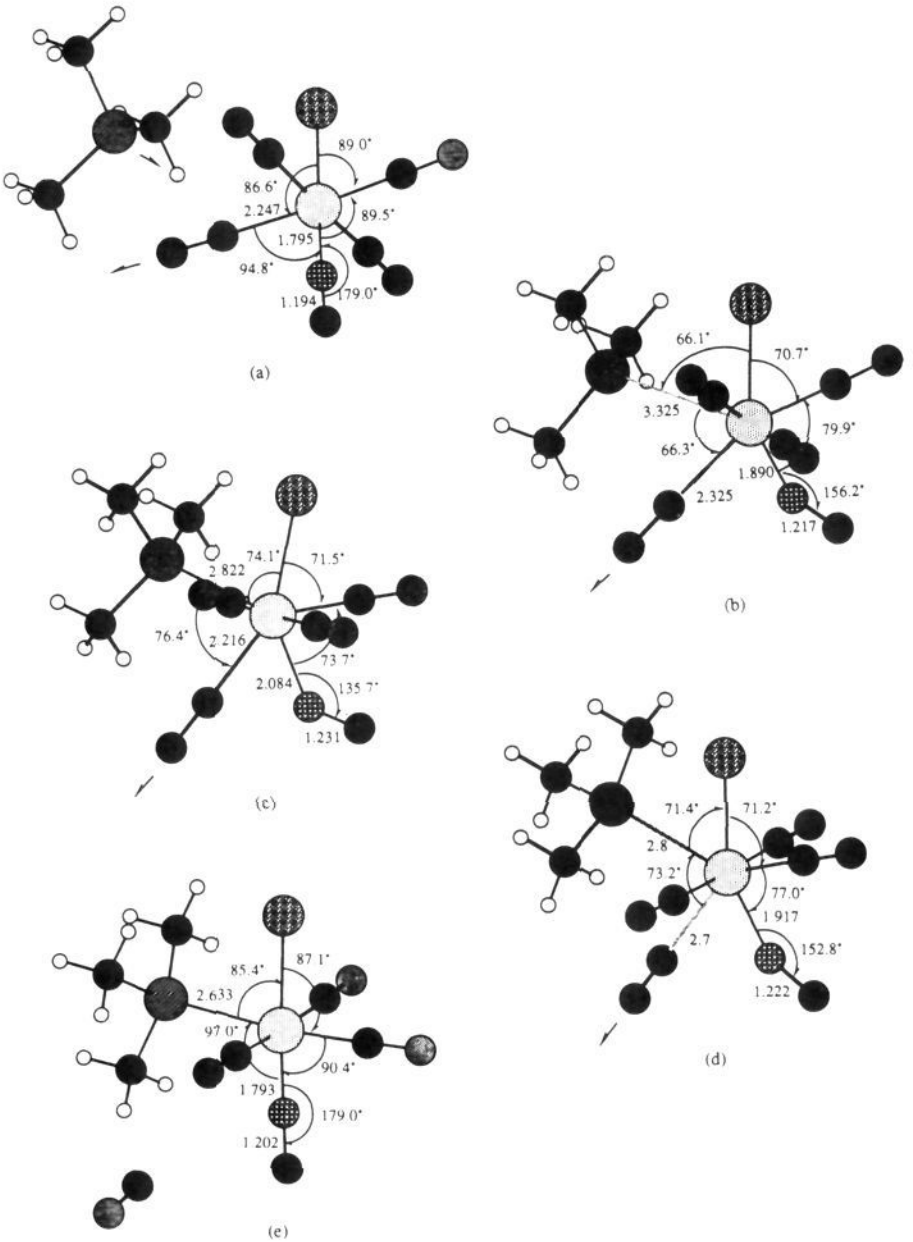

Figure 2. Optimized molecular geometries along the associative path: (a) reactant, (b) early transition state, (c) intermediate, (d) late transition state, (e) product for the CO substitution by PMe_3 in $W(CO)_4(NO)Cl$. Important structural parameters are in angstroms for bond distances and in degrees for bond angles.

eq 1, a detailed examination of the Laplacian of the charge distribution, $-\nabla^2\rho$, has been made. Figure 3 shows contour plots of $-\nabla^2\rho$ for the five structures (see Figure 2) along the reaction coordinate. To clarify the change of the charge distribution in the metal region, we also plot the valence-only Laplacian maps of the first three structures (see Figure 4), i.e., by removing the contribution from the W 5s and 5p electrons. The plots of $-\nabla^2\rho$ display regions of local charge concentration ($-\nabla^2\rho > 0$, denoted by solid contours) and local charge depletion ($-\nabla^2\rho < 0$, denoted by dashed contours). In this paper, all the contour maps of $-\nabla^2\rho$ were plotted in the mirror plane of the system discussed.

For the reactant, Figure 3a, there exist four maxima in the valence shell of charge concentration (VSCC) of the metal atom. These charge concentrations, which are located away from the bond paths that link the metal and donating atoms, correspond to nonbonded charge concentrations. Another significant charge concentration is the maximum in the VSCC of the nitrogen. Here the charge concentration is located on the W–N bond path and is part of the bonded charge concentration.

As the reaction proceeds to the early transition state, Figure 3b, some distinctive changes occur in the charge concentrations mentioned above. Responding to the approaching PMe_3 ligand, the nitrogen forms two maxima in its VSCC. The two maxima are located on either side of the linkage line between W and N. The larger maximum, which can be viewed as a nitrogen lone pair, moves away from the metal, while the smaller one is slightly closer to the metal. The critical point on the W–N bond path, q_c, is located off the linkage line between the W and N on the side of the smaller maximum. The angle between the W–N linkage and the W–q_c linkage, β, is 4.2°. Correspondingly, the nitrosyl ligand deviates from its linear geometry. In addition, significant changes also occur in the VSCC of the metal. As shown by comparing Figures 4a and 4b, the four nonbonded charge concentrations in the reactant disappear or decrease their extent in the early transition state, thus serving to accommodate the entering ligand and form a higher coordinate structure.

As the system evolves into the intermediate, more charge density concentrates in the area of the nitrogen lone pair and the nitrosyl

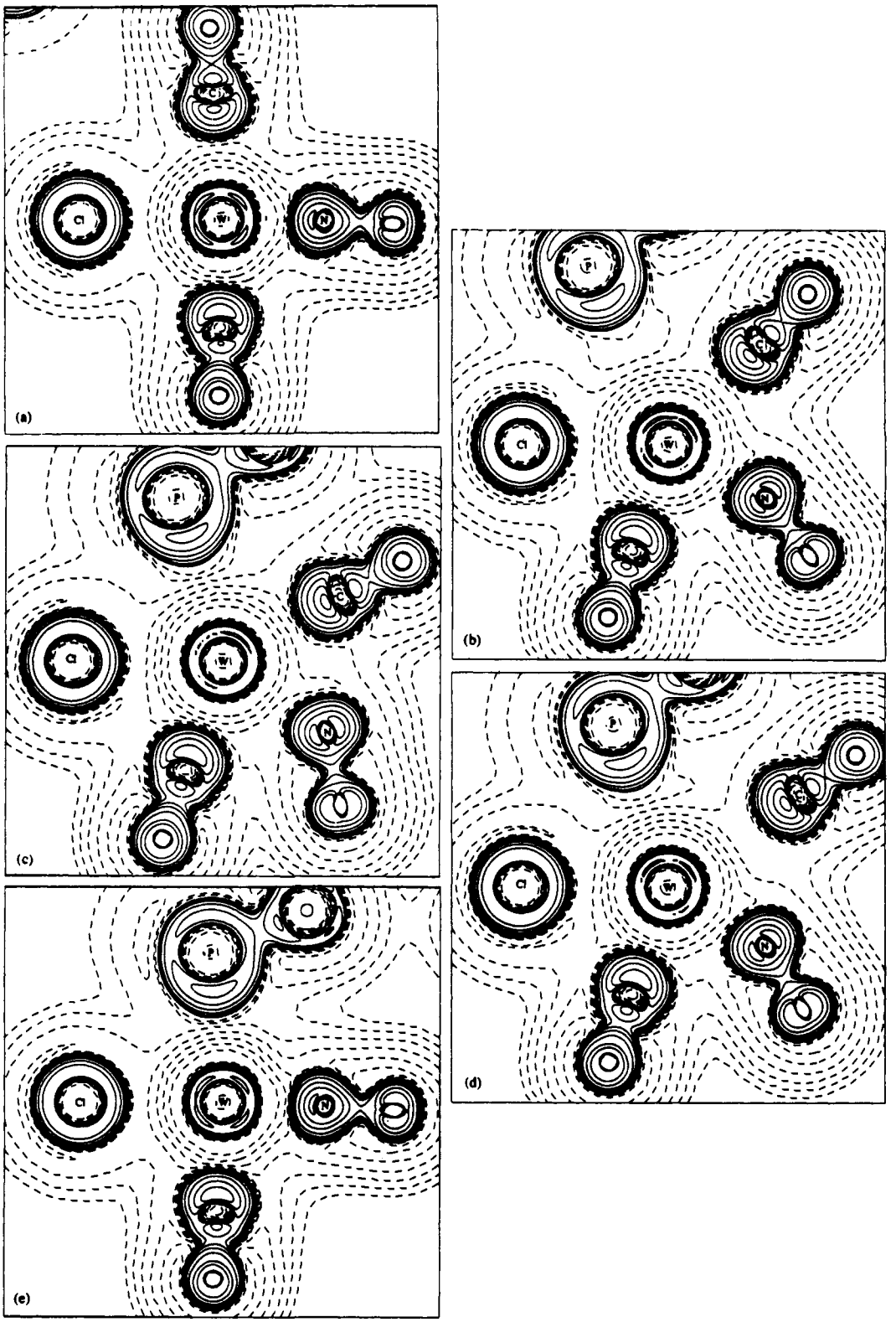

Figure 3. Contour plots of $-\nabla^2\rho$ for the five structures along the associative path: (a) reactant, (b) early transition state, (c) intermediate, (d) late transition state, (e) product for the CO substitution by PMe_3 in $W(CO)_4(NO)Cl$. Ten geometric contours of each sign are plotted. The absolute value of the smallest contour is 0.014 65 e/a_0.

ligand bends even more than it did in the early transition state. The angle β becomes 3.4° as the smaller maximum in the VSCC of the nitrogen turns toward the W–N linkage line. Around the metal, the nonbonded charge concentrations in the VSCC continue to disappear as shown in Figure 4c. Clearly, this redistribution of the charge density supports the interpretation that electrons shift to the nitrogen lone pair to vacate a coordinate site for the entering ligand.

A similar process in reverse order occurs in the last stage of the reaction (see Figures 3d and 3e). Finally, in the Laplacian map of the product (Figure 3e), four nonbonded charge concentrations reappear in the VSCC of the metal. Instead of the two maxima in the region of the nitrogen seen throughout the reaction, now only one bonded charge concentration points toward the metal center. The nitrosyl ligand has returned to a linear geometry with a short W–N bond.

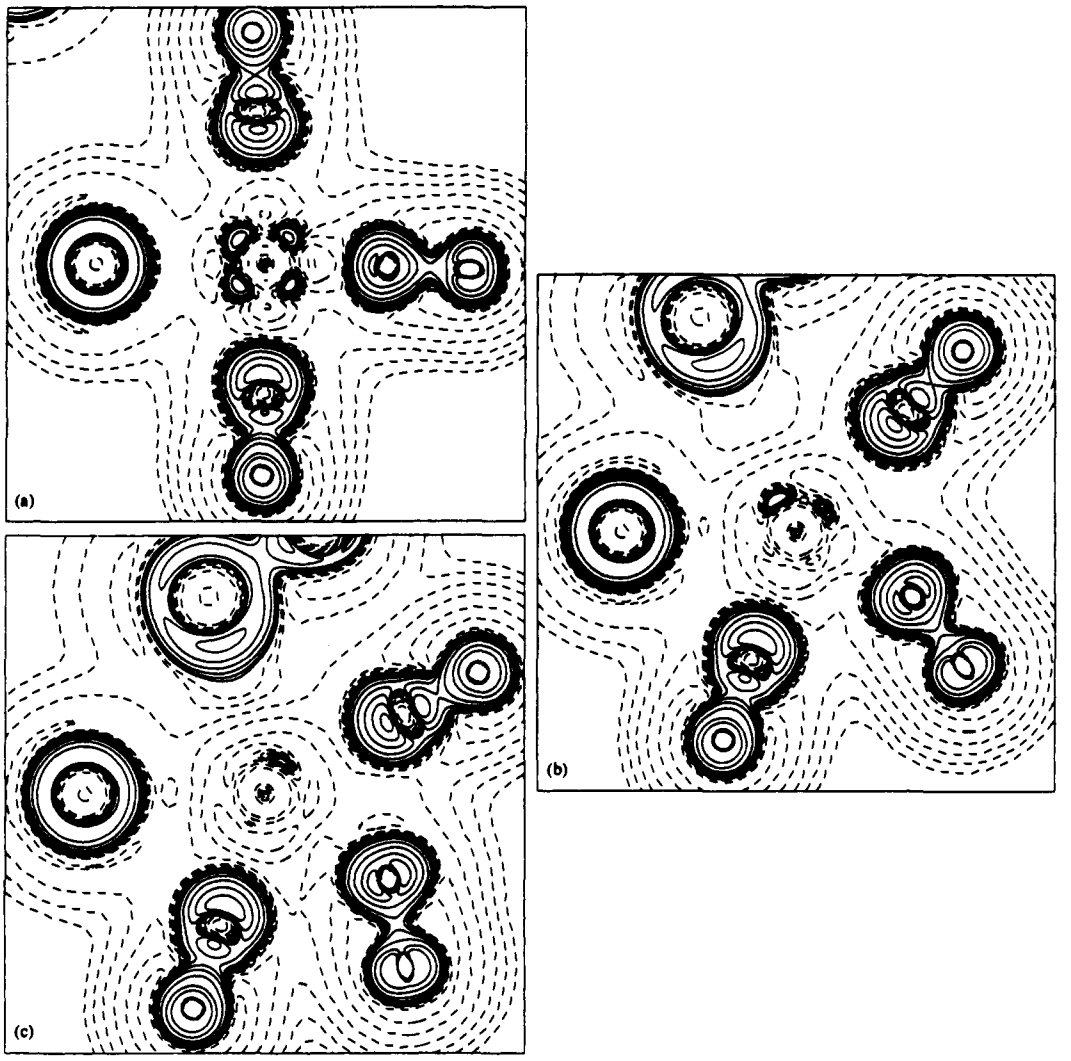

Figure 4. Contour plots of $-\nabla^2\rho_{\text{valence only}}$ for the first three structures along the associative path: (a) reactant, (b) early transition state, (c) intermediate for the CO substitution by PMe_3 in $W(CO)_4(NO)Cl$. Contour parameters are the same as in Figure 3.

The values of the charge density at the critical point (q_c) on the W–N bond path, ρ_c, provide complementary data on the strength of the W–N bond.[26] Table I shows the values of ρ_c corresponding to the five structures of Figure 2. Note that ρ_c decreases to its minimum (0.103) at the intermediate, which has the weakest W–N bond of the five structures. The above analyses clarify that through a geometric distortion the nitrosyl ligand plays a role of electron reservoir. This electron reservoir makes a crucial contribution by controlling the extent of the nonbonded interactions between the metal atom and the ligands.

CO Substitution by PH_3 in $W(CO)_4(NO)Cl$. Experimentally, an associative mechanism is not always the lower energy mechanism in CO substitution reactions of metal nitrosyl carbonyls. For example, although in CO substitution on $W(CO)_4(NO)X$ (X = Cl, Br, or I) the strong nucleophile $P(n\text{-}Bu)_3$ reacts through an associative mechanism, the poorer nucleophile PPh_3 reacts only through a dissociative mechanism.[10] Similar phenomena may occur in other CO substitutions of metal nitrosyl carbonyls.[1c] Considerable effort has been expended to quantify nucleophilic strengths of different phosphorus ligands.[3,4,27] We will not attempt a comprehensive investigation of this topic but rather provide some insight into the influence of nucleophilic strength on this reaction.

Table II. Electronic and Steric Data of Free PH_3 and PMe_3

	photoelectron data (eV)[a]	calculated HOMO (au)[b]	cone angle (deg)[c]
PH_3	10.58	−0.344 65	87
PMe_3	8.65	−0.287 50	118
difference	1.93	1.56 (eV)	

[a] Reference 28. [b] This work. [c] Reference 29.

For the purposes of this comparison, we employed PH_3 as an alternative entering ligand. Some important electronic and steric characteristics of free PMe_3 and PH_3 are summarized in Table II.[28,29] Since it has a higher energy HOMO and its cone angle is not significantly larger, PMe_3 is a better electron donor than PH_3. We will see below that replacing PMe_3 with PH_3 causes significant changes in the reaction mechanism.

Figure 5 presents the potential energy surface and contour plot for CO substitution by PH_3 on $W(CO)_4(NO)Cl$. To compare the PH_3 and PMe_3 substitutions, Figure 6 shows two representative energy profiles, which were obtained by cutting the potential energy surfaces in Figures 1 and 5 along the coordinate R_2 at R_1 = −0.5 Å. For PMe_3, an energy minimum is observable close to R_2 = 5.0 Å (R_{W-C_c} = 2.25 Å, R_{W-P} = 2.75 Å); this minimum corresponds to the region of the intermediate in the associative

(26) Bader, R. F. W.; Slee, T. S.; Cremer, D.; Kraka, E. *J. Am. Chem. Soc.* **1983**, *105*, 5061.

(27) (a) Streuli, C. A. *Anal. Chem.* **1960**, *32*, 985. (b) Tolman, C. A. *Chem. Rev.* **1977**, *77*, 313. (c) Rahman, M. M.; Liu, H. Y.; Prock, A.; Giering, W. P. *Organometallics* **1987**, *6*, 650. (d) Bush, R. C.; Angelici, R. J. *Inorg. Chem.* **1988**, *27*, 681. (e) Poe, A. J. *Pure Appl. Chem.* **1988**, *60*, 1209 and references therein.

(28) Stelzer, O.; Unger, E. *Chem. Ber.* **1975**, *108*, 1246.

(29) Tolman, C. A. *J. Am. Chem. Soc.* **1970**, *92*, 2956.

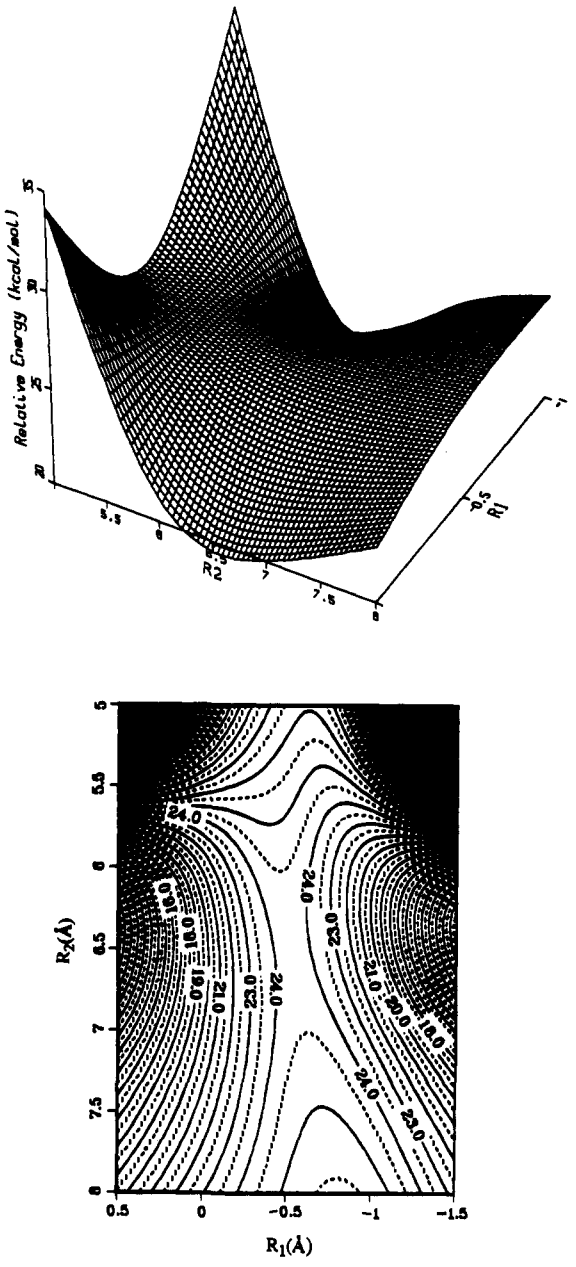

Figure 5. Potential energy surface and contour plot for the CO substitution by PH_3 in $W(CO)_4(NO)Cl$ as a function of the R_1 and R_2 distances. Energies are in units of kcal/mol.

mechanism. In contrast, only a very shallow energy minimum exists on the curve for PH_3 at about R_2 = 6.5 Å (R_{W-C_c} = 3.0 Å, R_{W-P} = 3.5 Å); this species corresponds to a fragment with two dissociated ligands. Therefore, the PH_3 substitution proceeds by a dissociative or I_d mechanism.

It is noteworthy that the PH_3 reaction system still gives a bent nitrosyl geometry in the short region of R_2. For example, the structure S_H at R_2 = 5.0 Å on the PH_3 curve (see Figure 6) exhibits a W–N–O angle of 136.5°, while the corresponding structure S_{Me} on the PMe_3 curve displays a W–N–O angle of 135.9°. Even though the nitrosyl bends strongly, it is unable to provide a low-energy associative path for the PH_3 substitution. To resolve this dilemma, we compared the electronic structures of the PH_3 and PMe_3 reaction systems by plotting, as contour plots, the deformation density of the complexes. The deformation density (Figure 7) was plotted in the mirror plane of the complex by subtracting the densities of the promolecules, the PR_3 and $W(CO)_4(NO)Cl$ fragments, from the total density of the molecule. Figures 7a and 7b show the deformation density at S_H and S_{Me}*, respectively. The latter was formed by fixing the geometry of

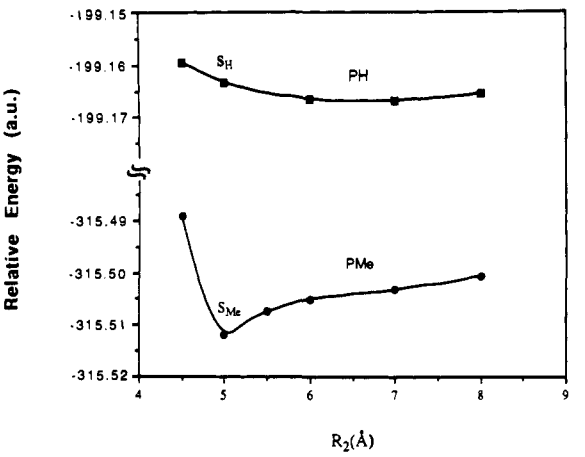

Figure 6. Potential energy curves for the CO substitutions by PH_3 and by PMe_3 in $W(CO)_4(NO)Cl$ as a function of R_2 at R_1 = –0.5 Å.

the complex S_H but replacing the PH_3 ligand with the PMe_3 ligand. The only structural difference between S_H and S_{Me}* is the change in the nucleophile from PH_3 to PMe_3. Thus, we can compare the pure electronic effects caused by different nucleophiles.

As shown in Figure 7, the PMe_3 ligand donates more electron density to the metal fragment than the PH_3 ligand does. Also, for the complex S_{Me}*, more electron density accumulates in the bonding regions between the W atom and ligands, particularly between the W and PMe_3 as well as between the W and NO. Therefore, one can understand the electronic effect of a nucleophile in the following way. With the bending of the NO ligand, the reaction system becomes destabilized due to the weakening of the W–N bond. A better electron donor can reduce this destabilization by strengthening the M–P bond and the M–N single bond. If the incoming nucleophile is strong enough, a relatively low-energy system will result; otherwise, although a coordinate site could be vacated through the bending of the NO ligand, it will not bend and an associative mechanism will not be accessible.

We can arrange the following four nucleophiles in the descending order of strength[27]

$$P(n\text{-}Bu)_3 \sim P(Me)_3 > PPh_3 > PH_3$$

Since PMe_3 and PH_3 should qualitatively model the behavior of the bulky phosphorus nucleophiles $P(n\text{-}Bu)_3$ and PPh_3, respectively, our results for CO substitution by PMe_3 (or PH_3) are in essential agreement with the experimental findings.[10]

CO Substitution by PH_3 in $Re(CO)_5Cl$. To understand better the unique contribution of the nitrosyl ligand to the associative mechanism, we performed parallel calculations on the substitution reaction of the isoelectronic metal carbonyl $Re(CO)_5Cl$ (**2**). Figure 8 shows the corresponding potential energy surface and contour plot.

Consistent with the experiment result,[11] an associative mechanism is not predicted by the potential energy surface of the rhenium complex. Interestingly, the C_NO_N ligand in **2**, which corresponds to the nitrosyl ligand in **1**, stays linear (largest deviation of 7.8°) even when the reaction system is forced into the 7-coordinate region. For comparison of the PH_3 substitutions in the tungsten and rhenium systems, two representative structures as well as the corresponding Laplacian maps are shown in Figure 9. Both structures are located at R_1 = –0.5 Å and R_2 = 5.0 Å on their respective potential energy surfaces (Figures 5 and 8). As shown in Figure 9, the nitrosyl ligand in the tungsten complex bends significantly to 136.5°, while the C_NO_N ligand in the rhenium complex bends only slightly to 173.5°. A marked difference is also observable in the electron density distribution of the two complexes. In contrast to the two maxima in the VSCC of the nitrogen (see Figure 9a′), only a single charge concentration appears in the VSCC of the C_N (see Figure 9b′). In the VSCC of the rhenium, unlike tungsten, the four strong nonbonded charge concentrations of the original 6-coordinate system remain. Since

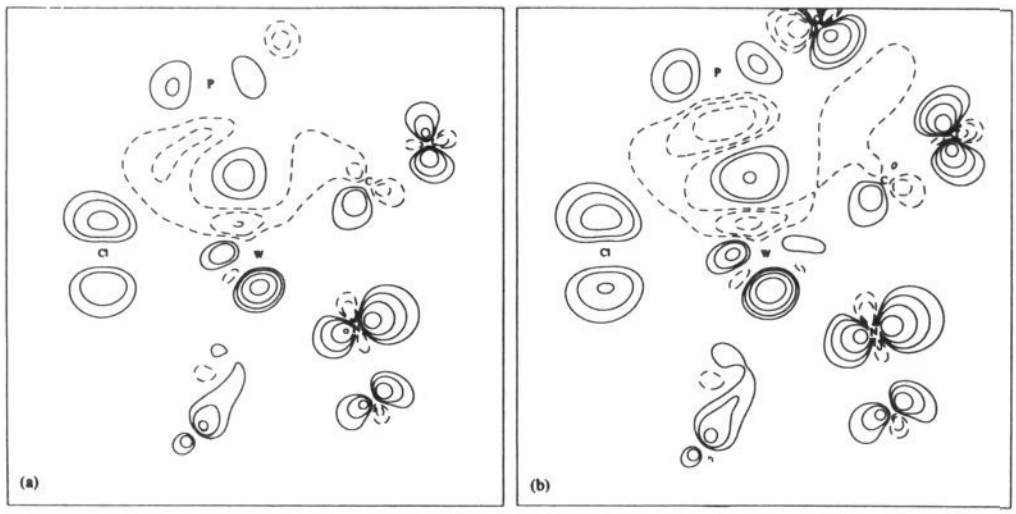

Figure 7. Plots of deformation density for the complexes: (a) S_H (see Figure 6); (b) S_{Me}* (obtained by replacing the PH_3 in S_H with PMe_3). The plots are gained by subtracting the electron densities of the promolecules PH_3 (or PMe_3) and $W(CO)_4(NO)Cl$ from the total density of the molecule. Adjacent lines differ by a factor of 2. The lowest contour is 0.001 95 e/au^3.

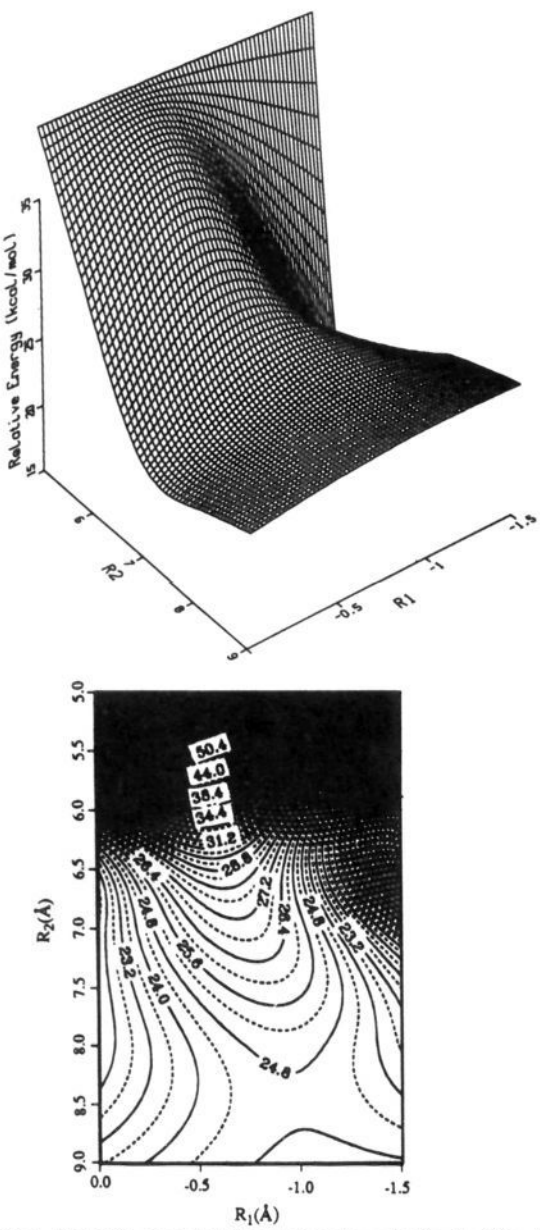

Figure 8. Potential energy surface and contour plot for the CO substitution by PH_3 in $Re(CO)_5Cl$ as a function of the R_1 and R_2 distances. Energies are in units of kcal/mol.

the four nonbonded concentrations cannot properly avoid the five donating ligands, the repulsion between the Re and the ligands leads to a very unstable system (see the corresponding contour value of Figure 8). To reduce the metal–ligand repulsion, the reaction system would rather keep the entering and leaving ligands far from the Re center, leading to a dissociative reaction mechanism.

The difference in behavior of nitrosyl and carbonyl reflects an essential distinction in their electronic structure. For nitrosyl, the ground-state configuration is π^*.[1] This low-energy, singly occupied π^* orbital contributes much to the stability of a bent nitrosyl. According to Hoffmann et al.,[30] one of the important factors in stabilizing a bent nitrosyl geometry is the σ-like interaction between a metal d orbital and the NO π^* orbital in a bent nitrosyl complex. A similar stabilizing interaction, which is depicted in **3**, dominates the HOMO of the intermediate (Figure 2c). This

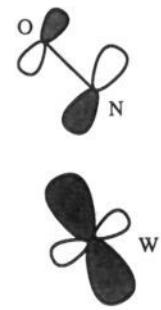

3

bonding interaction moves an electron pair from the metal to the nitrogen lone pair and makes up for the loss of the W–N donor bond in a bent nitrosyl structure. In contrast, due to its high energy the π^* orbital of carbonyl cannot contribute in the same fashion to stabilize the occupied orbitals of the rhenium complex. Thus, the reaction system cannot benefit through a bending of the C_NO_N ligand. The calculations suggest that the C_NO_N ligand tends to remain linear in order to retain its only possible strong bond, the Re–C donor bond.

Influence of Basis Set. The calculations of the potential energy surfaces reproduced the principal features of the experiments; thus, our calculations must provide, at least, a reasonably accurate representation of the electronic features of these reactions. In the calculations discussed above, we used single-ζ basis sets and

(30) Hoffmann, R.; Chen, M. M. L.; Elian, M.; Rossi, A. R.; Mingos, D. M. P. *Inorg. Chem.* **1974**, *13*, 2666.

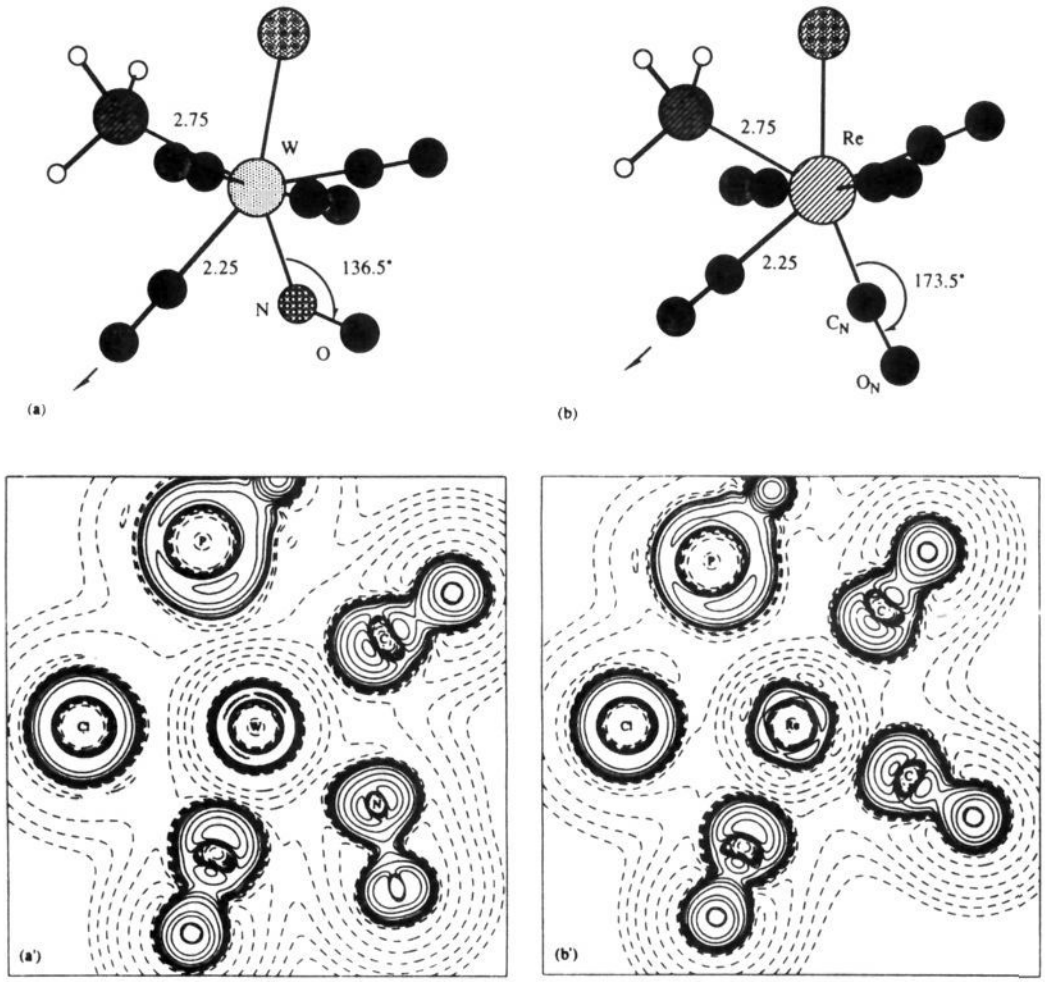

Figure 9. Optimized molecular geometries and contour plots of $-\nabla^2\rho$ at $R_1 = -0.5$ Å, $R_2 = 5.0$ Å for the CO substitutions by PH_3 in $W(CO)_4(NO)Cl$ (a and a′) and in $Re(CO)_5Cl$ (b and b′). Structural parameters are in angstroms for bond distances and in degrees for bond angles. Contour parameters are the same as in Figure 3.

fixed metal–ligand bond lengths for the spectator ligands in constructing the potential energy surfaces. In the additional calculations discussed below, we relaxed all the metal–ligand bond distances in **1** and used an enlarged basis set, in which all the basis functions were represented in a double-ζ form except those of the Me groups. Figure 10 presents both the new and previous results. All curves are along the coordinate R_2 at $R_1 = -0.5$ Å. Curves labeled PH^a and PMe^a correspond to substitution reactions in the larger basis, while curves labeled PH and PMe correspond to the reactions in the smaller basis.

As shown in Figure 10, both basis sets display similar trends. The calculations with larger basis sets give additional support to the conclusions that the PMe_3 substitution proceeds by an associative (A) mechanism, while the PH_3 substitution proceeds by a dissociative (D) mechanism. We also noted that for the PH_3 substitution, the calculations with the smaller basis set PH suggest an I_d mechanism, which is indicated by a local minimum on the PH_3 curve, while the calculations with the larger basis set PH^a remove this minimum and predict a D mechanism.

Electron Correlation Effects. It has been shown that the inclusion of electron correlation effects is essential for some transition-metal nitrosyl complexes.[31] Indeed, the influence of electron correlation is reflected in our RHF results. As presented in Figure 2, for the PMe_3 substitution of $W(CO)_4(NO)Cl$ the W–N bond lengths of reactant and product are 1.795 Å and 1.793 Å, respectively. They are significantly shorter than the experimental value of 1.873 Å in $(PhMe_2P)_2WI(CO)_2(NO)$.[10] In addition, we found that the wave functions for the five structures in Figure 2 contain a high-energy occupied metal–nitrosyl π-bonding orbital and a low-energy metal–nitrosyl antibonding virtual orbital. Therefore, the geometry optimizations at the correlated level may elongate the W–N bond by the excitations from the high-energy occupied metal–nitrosyl π-bonding orbital to the low-energy metal–nitrosyl antibonding virtual orbital. Thus, the W–N bond distance changes predicted above must be viewed with some caution.

Since CI techniques such as CASSCF or MCSCF methods are too time-consuming for these problems, we turn to a simple configuration interaction with single and double excitations (CISD) as a method for examining electron correlation effects. CISD calculations with 88 molecular orbitals and 72 electrons were carried out for the PH_3 reaction with $W(CO)_4(NO)Cl$ along R_1 at $R_2 = 7.0$ Å and along R_2 at $R_1 = -0.5$ Å, respectively. For the CISD calculations, the reference configuration and molecular structure were taken from the potential energy surface in Figure 5. The resulting CISD curves and corresponding RHF results are compared in Figure 11.

Along coordinate R_1 (from reactant to product through the I_d region) the CISD and RHF calculations have quite similar energy curves (see the CISD(1) and RHF(1) curves in Figure 11), while along coordinate R_2 (along the intermediate/transition-state region from the A to I_d to D region), the CISD calculations have significantly shifted the potential energy surface toward larger values

(31) (a) Fenske, R. F.; Jensen, J. R. *J. Chem. Phys.* **1979**, *71*, 3374. (b) Bursten, B. E.; Jensen, J. R.; Gordon, D. J.; Treichel, P. M.; Fenske, R. F. *J. Am. Chem. Soc.* **1981**, *103*, 5227. (c) Mougenot, P.; Demuynck, J.; Benard, M. *J. Phys. Chem.* **1988**, *92*, 571.

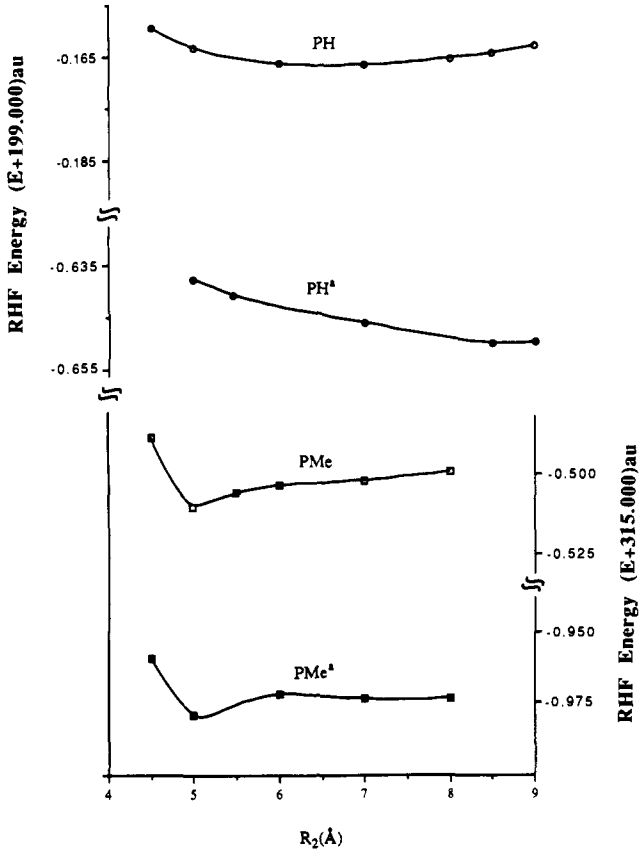

Figure 10. Potential energy curves along R_2 at $R_1 = -0.5$ Å for the CO substitutions in $W(CO)_4(NO)Cl$: PH and PH^a by PH_3; PMe and PMe^a by PMe_3. Larger basis sets and more optimization parameters were used for the curves PH^a and PMe^a, while smaller basis sets and less optimization parameters were used for the curves PH and PMe.

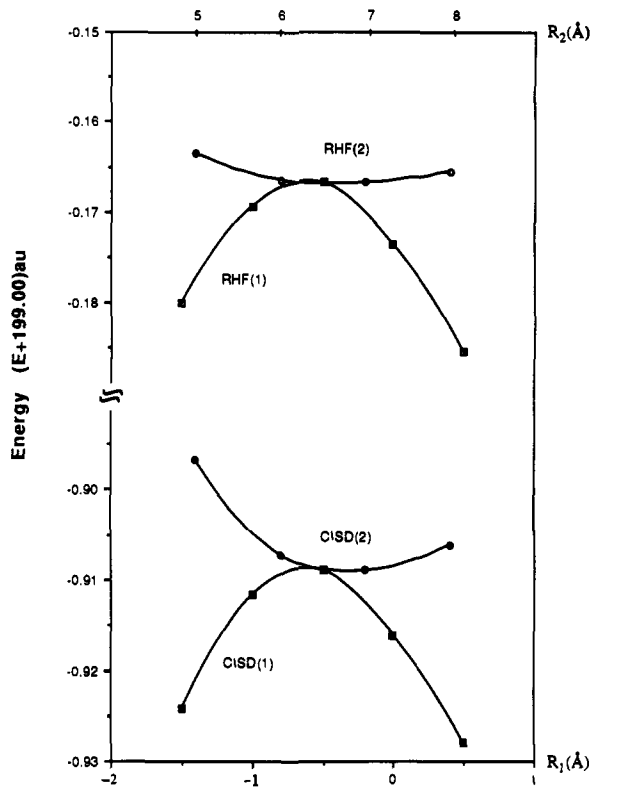

Figure 11. RHF and CISD potential energy curves along R_1 at $R_2 = 7.0$ Å (RHF(1) and CISD(1)) and along R_2 at $R_1 = -0.5$ Å (RHF(2) and CISD(2)) for the CO substitutions by PH_3 in $W(CO)_4(NO)Cl$.

of the R_2 (see the CISD(2) and RHF(2) curves in Figure 11). The curve shifting that occurs along coordinate R_2 probably is due to the fact that the CISD calculations tend to elongate both the W–C and W–P bonds. Therefore, the CISD calculations qualitatively support the RHF results. On the other hand, relative to the RHF(2) curve, the CISD(2) curve has a deeper local minimum. However, since the calculations with a larger basis set tend to remove the local minimum at the RHF level, we could only speculate what would happen in a very large basis set at a high level of CI. We can conclude that the dissociative reaction region is a basis set- and correlation-sensitive system; thus the question of a dissociative vs an I_d mechanism for PH_3 remains open.

Conclusions

Through the construction of ab initio potential energy surfaces, we predicted an associative mechanism with a seven-coordinate intermediate for the substitution by PMe_3 on $W(CO)_4(NO)Cl$. The intermediate has a bent nitrosyl ligand with a W–N–O bond angle of 135.7°. The analysis on the charge density distribution of the reaction system supports the interpretation that electrons shift to the nitrogen lone pair to vacate a coordinate site for the entering ligand.

This geometry distortion and electron shift are not available in the CO substitution of $Re(CO)_5Cl$. As a result, the substitution in the rhenium system proceeds by a dissociative or I_d mechanism. The relative strength of the attacking nucleophile also contributes much to the appearance of an associative mechanism. In contrast to PMe_3, the poorer donor PH_3 is unable to stabilize the 7-coordinate intermediate and its CO substitution in $W(CO)_4(NO)Cl$ proceeds by an I_d or D mechanism.

Acknowledgment. The authors thank the National Science Foundation (Grants No. CHE 86-19420 and 91-13634) and the Robert A. Welch Foundation (Grant No. A-648) for financial support. This research was conducted in part using the Cornell National Supercomputer Facility, a resource of the Center for Theory and Simulation in Science and Engineering at Cornell University, which is funded in part by the National Science Foundation, New York State, and the IBM Corporation. We also thank Cray Research for a grant of computer time on the CRAY Y-MP2/116 at the Supercomputer Center of Texas A&M University.